Nat. Hazards Earth Syst. Sci., 15, 2183–2200, 2015
www.nat-hazards-earth-syst-sci.net/15/2183/2015/
doi:10.5194/nhess-15-2183-2015

Natural Hazards and Earth System Sciences
Open Access

Large submarine earthquakes that occurred worldwide in a 1-year period (June 2013 to June 2014) – a contribution to the understanding of tsunamigenic potential

R. Omira[1,2], D. Vales[1], C. Marreiros[1], and F. Carrilho[1]

[1]Instituto Português do Mar e da Atmosfera, IPMA, IP, Lisbon, Portugal
[2]Instituto Dom Luiz, University of Lisbon, IDL, Lisbon, Portugal

Correspondence to: R. Omira (omirarachid10@yahoo.fr)

Received: 19 February 2015 – Published in Nat. Hazards Earth Syst. Sci. Discuss.: 11 March 2015
Revised: 18 September 2015 – Accepted: 21 September 2015 – Published: 7 October 2015

Abstract. This paper is a contribution to a better understanding of the tsunamigenic potential of large submarine earthquakes. Here, we analyze the tsunamigenic potential of large earthquakes which have occurred worldwide with magnitudes around $M_w = 7.0$ and greater during a period of 1 year, from June 2013 to June 2014. The analysis involves earthquake model evaluation, tsunami numerical modeling, and sensors' records analysis in order to confirm the generation of a tsunami (or lack thereof) following the occurrence of an earthquake. We also investigate and discuss the sensitivity of tsunami generation to the earthquake parameters recognized to control tsunami occurrence, including the earthquake location, magnitude, focal mechanism and fault rupture depth. Through this analysis, we attempt to understand why some earthquakes trigger tsunamis and others do not, and how the earthquake source parameters are related to the potential of tsunami generation. We further discuss the performance of tsunami warning systems in detecting tsunamis and disseminating the alerts. A total of 23 events, with magnitudes ranging from $M_w = 6.7$ to $M_w = 8.1$, have been analyzed. This study shows that about 39 % of the analyzed earthquakes caused tsunamis that were recorded by different sensors with wave amplitudes varying from a few centimeters to about 2 m. Tsunami numerical modeling shows good agreement between simulated waveforms and recorded waveforms, for some events. On the other hand, simulations of tsunami generation predict that some of the events, considered as non-tsunamigenic, caused small tsunamis. We find that most generated tsunamis were caused by shallow earthquakes (depth < 30 km) and thrust faults that took place on/near the subduction zones. The results of this study can help the development of modified and improved versions of tsunami decision matrixes for various oceanic domains.

1 Introduction

In the aftermath of the 2004 Indian Ocean tsunami, much effort has been made worldwide to better understand the potential of tsunami generation following the occurrence of an earthquake. As a result, various research studies have been carried out in order to (i) identify the source zones most prone to triggering tsunamis around the world, (ii) understand the generation mechanism of tsunami sources, (iii) assess tsunami hazard, vulnerability, and risk along coastal areas, (iv) reinforce the existing tsunami warning systems (TWSs) and implement new ones and (v) improve the capability of tsunami warning centers (TWCs) to detect the tsunami well before it hits the coastal zones. One issue that remains challenging for any TWC, in order to avoid false warning and to mitigate the tsunami impact on the coastal population, is the fast confirmation of the generation of a tsunami (or lack thereof) after the occurrence of an earthquake. Solving such an issue, in particular with the absence of tsunami detection sensors deployed close to the earthquake epicenter, remains a hard task and requires robust knowledge on the geology, tectonics and geodynamics of the region where the earthquakes are generated in addition to robust tsunami numerical modeling capabilities to simulate the different phases of a tsunami properly.

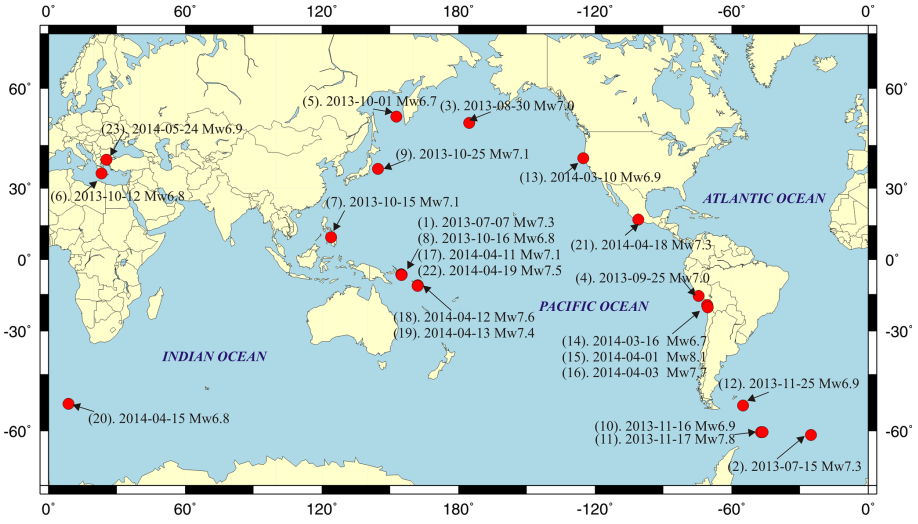

Figure 1. Locations of the epicenters (red dots), event number (given in Table 1), date of occurrence and magnitudes of submarine earthquake events of $M_w >= 6.7$ that were analyzed during a 1-year period from June 2013 to June 2014.

In general, various parameters are recognized to control the generation of a tsunami following an earthquake event. These parameters mainly include the earthquake magnitude, its location, its focal mechanism and its rupture depth. The available tsunami database from 2000 BC to present (NGDC/WDS, 2014) shows that among the total of 1425 tsunami historical events, 80 % were caused by earthquakes of magnitude greater than $M_w = 6.5$. Most, but not all, known devastating tsunamis has been caused by earthquakes triggered in subduction zones. According to Satake and Tanioka (1999), tsunamigenic earthquakes in subduction zones can be classified into three types: (i) typical interplate events, which occur at the plate interface; (ii) intraplate events concerning earthquakes at the outer-rise within the subducting slab or overlying crust; and (iii) "tsunami earthquakes" that take place at the shallow extension of the interplate seismogenic zone, typically beneath the accretionary wedge.

This study aims to contribute to a better understanding of tsunamigenic potential from sources of tectonic origin by analyzing the tsunami generation associated with large earthquakes that occurred worldwide during a period of 1 year. 23 submarine earthquake events of magnitudes ranging from $M_w = 6.7$ up to $M_w = 8.1$ have been analyzed (Fig. 1). The period of 1 year seems to be short to conduct a comprehensive analysis, especially from a statistical point of view. On the other hand, due to the fact that during the considered period, 23 events occurred in different regions of the world with various focal mechanisms and rupture conditions, we assume that a 1-year period provides enough data to cover the scope of this paper, which does not include a statistical analysis.

Most considered events occurred in the Pacific Ocean on/near the plate subduction zones. These events took place with different focal mechanisms of generation and different earthquake hypocenter depths. The analysis performed in this study involves source parameters evaluation, tsunami numerical modeling of generation and propagation, and sensors' records, including coastal tide gauges (TD), and "Deep-ocean Assessment and Reporting of Tsunamis" (DART®), that serve to confirm the generation (or lack thereof) of a tsunami. With this analysis, we attempt to understand why some earthquakes cause tsunamis and others do not, and how the source parameters are related to the potential of tsunami generation. Definition of source parameters includes the earthquake epicenter location (from USGS, http://earthquake.usgs.gov/earthquakes/), its magnitude, its depth, and its focal mechanism, which are available by the gCMT (Global Centroid-Moment-Tensor, http://www.globalcmt.org/) after the event occurrence. To evaluate the additional parameters, such as the fault dimensions (L, W) and the average coseismic slip (D), required for tsunami numerical modeling, we use the earthquake scaling laws Mw-L/W and Mw-D established by Blaser et al. (2010). To simulate the possible initial sea-surface perturbation, the earthquake rupture is supposed instantaneous and the sea-bed displacement is computed using the half-space elastic theory (Okada, 1985). The tsunami propagation is modeled using the COMCOT finite-differences shallow water code (Liu et al., 1998).

Analysis of available sensor records reveals that 39 % of the considered earthquakes caused tsunamis. Tsunamis caused by non-seismic events, such as the 24 September 2013 tsunami, possibly associated to submarine landslide (Heidarzadeh and Satake, 2014), that occurred following the $M_w = 7.7$ inland Pakistan earthquake and recorded by TD stations along the Omani coast, are disregarded in our study. We discuss how various specific characteristics of the studied earthquakes and their mechanisms of gener-

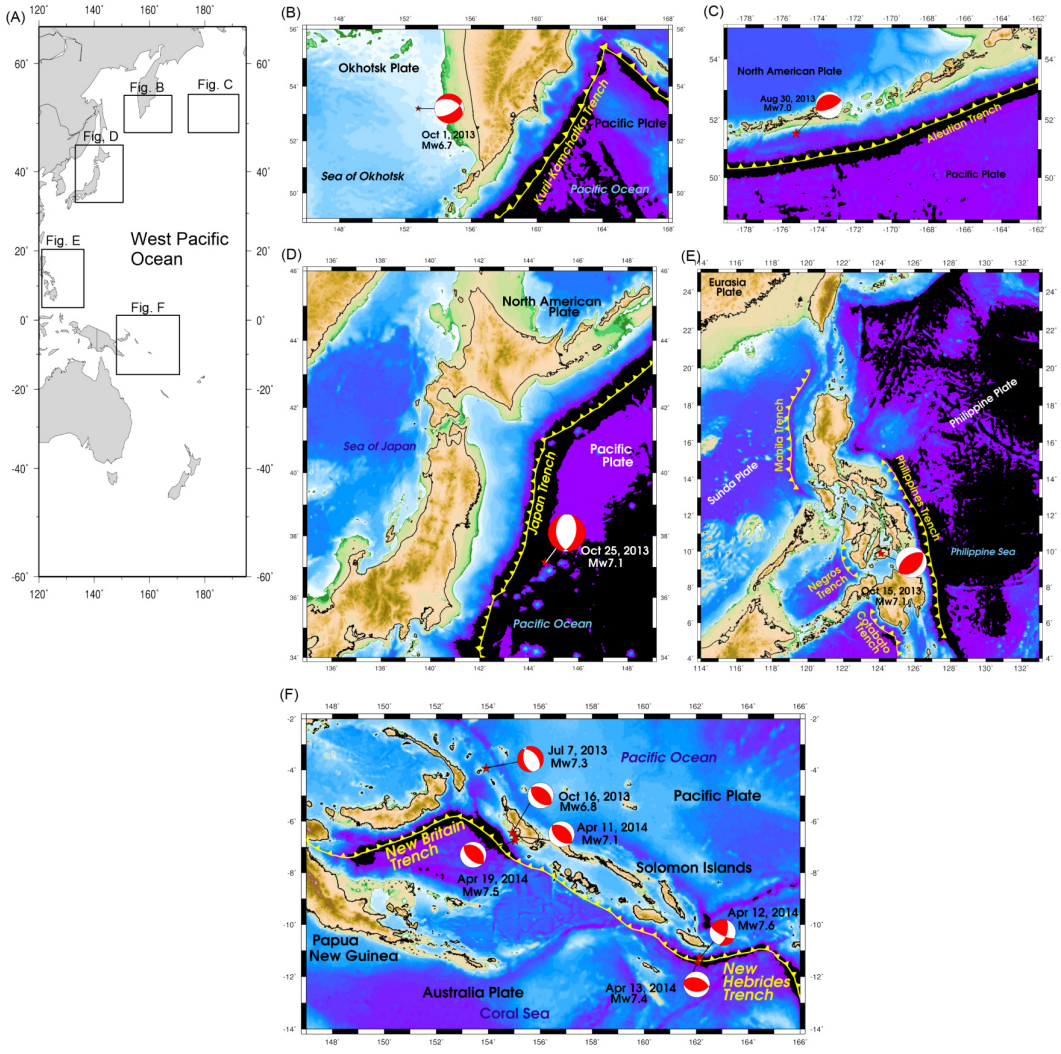

Figure 2. Earthquake events which occurred in the west Pacific source zone: **(a)** overview of the source zone; location of the epicenters (red stars), focal mechanisms (red beach balls), and subduction zones (yellow lines) for: **(b)** the Okhotsk-Russia normal faulting event, **(c)** the Alaska thrust fault event, **(d)** the Honshu normal faulting event, **(e)** the Philippine reverse faulting event, and **(f)** six events, four around the Papua New Guinea, their focal mechanisms: three are normal faulting and one is thrust faulting, and two near the Solomon Island, their focal mechanisms: a strike–slip and a reverse faulting.

ation, such as the earthquake magnitude, the location, the type of focal mechanism and the depth of the rupture determine their tsunamigenic potential. 67 % of caused tsunamis resulted from thrust faults that occurred in/near subduction zones. We finally highlight the performance of the different TWSs around the world related to the triggered tsunami events and discuss, in light of the paper results, some earthquake characteristics that can be considered in order to improve the tsunami decision matrixes for various oceanic domains.

2 Earthquake events: tectonic setting and focal mechanisms

In this study 23 large submarine earthquakes, which occurred between June 2013 and June 2014, have been considered. Assessing the tsunamigenic potential of the studied earthquakes requires an understanding of the tectonic setting of the regions where these events occurred. Here, we describe these settings along with the focal mechanism of each earthquake. We consider four main source zones (SZs) as responsible for the generation of the studied events. They are: the west Pacific (Fig. 2), the east Pacific (Fig. 3), the South Atlantic (Fig. 4) and the east Mediterranean (Fig. 5) SZs.

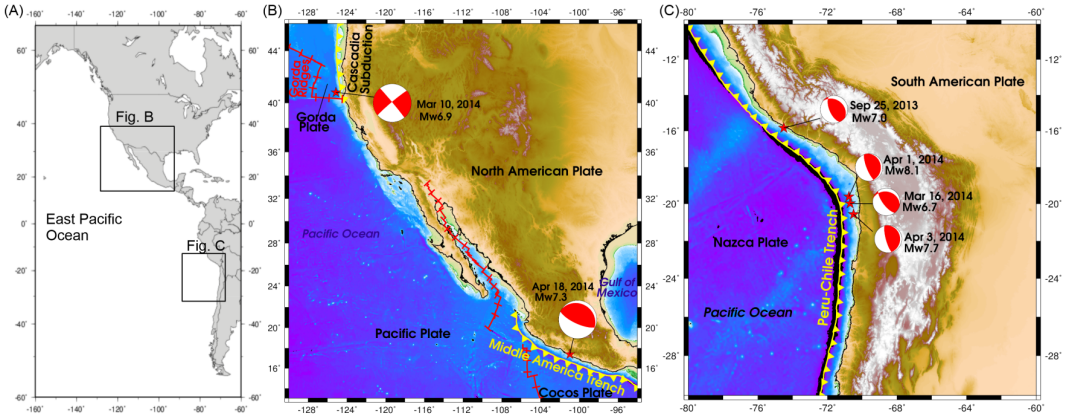

Figure 3. Earthquake events which occurred in the east Pacific source zone: **(a)** overview of the source zone; **(b)** location of the California and Mexico events (red stars), their focal mechanism: thrust faulting and strike–slip faulting, respectively (red beach ball), the subduction zone (yellow line) and the spreading centers (red lines); **(c)** location of four events: the Peru event and three events in northern Chile (red stars), their focal mechanisms are thrust faulting (red beach ball), and the subduction zone (yellow line).

In the west Pacific SZ, 10 events occurred (Fig. 2). In the Sea of Okhotsk, on 1 October 2013, a $M_w = 6.7$ earthquake was the result of normal faulting at a depth of 585 km. Its location was close to the region where the Pacific Plate subducts beneath the Okhotsk Plate (Fig. 2b). In the Aleutian Islands region, a $M_w = 7.0$ earthquake took place on 30 August 2013 at a depth of 26.7 km, as the result of thrust faulting on/near the Aleutian Trench (Fig. 2c). Offshore of Honshu, Japan, a $M_w = 7.1$ earthquake occurred on 25 October 2013, associated with normal faulting in the oceanic crust of the Pacific Plate, east of the Japan Trench (Fig. 2d). In the Bohol Islands, Philippines, on 15 October 2013, a $M_w = 7.1$ earthquake (Fig. 2e) was generated by a previously unmapped reverse fault (Lagmay and Eco, 2014). The depth of the event (12 km) indicates that it ruptured a fault within the crust of the Sunda Plate, rather than on the deeper subduction zone plate boundary. Four events occurred in Papua New Guinea (Fig. 2f) within two tectonic regions: the Australian slab and the New Britain Trench. The Australian slab was responsible for the generation, on 7 July 2013, of a $M_w = 7.3$ earthquake associated with normal faulting at 385 km depth. Close to the New Britain Trench, three other earthquakes (Fig. 2e) were the result of thrust faulting on the Australia–Pacific subduction zone. They took place on 16 October 2013, 11 April 2014 and 19 April 2014 with $M_w = 6.8$, $M_w = 7.1$ and $M_w = 7.5$ at depths of 45.8, 44.1 and 36 km, respectively. In the Solomon Islands, two earthquakes happened on 12 April 2014, and 13 April 2014 with $M_w = 7.6$ and $M_w = 7.4$, respectively, along a segment of the Australia–Pacific Plate boundary (Fig. 2f). The first event was a strike–slip earthquake, while the second was nearly a pure reverse.

In the east Pacific SZ, six events occurred (Fig. 3). On 10 March 2014, a $M_w = 6.9$ earthquake occurred off the coast of northern California, resulting from a strike–slip motion in a region where the Gorda Plate subducts beneath the Pacific northwest region (Fig. 3b). On 18 April 2014, a $M_w = 7.3$ earthquake happened near the Pacific coast of Mexico (Fig. 3b) as the result of thrust motion at a shallow depth (18.9 km). On 25 September 2013, a $M_w = 7.0$ earthquake occurred off the coast of Peru at 46.1 km depth because of thrust faulting on/near the interface at the boundary between the South American Plate and the subducting Nazca Plate (Fig. 3c). Just off the Chilean coast, three earthquakes resultant of thrust faulting, at shallow depths of 12, 21.6 and 28.7 km, occurred in the subduction zone along which the Nazca Plate underthrusts the South American Plate (Lay et al., 2014) (Fig. 3c). The first event, on 16 March 2014, with $M_w = 6.7$, was considered as a foreshock of the 1 April 2014 $M_w = 8.1$ event, and the 3 April 2014 $M_w = 7.7$ event was an aftershock.

In the South Atlantic SZ, five events occurred (Fig. 4). At the South Sandwich Islands one strike–slip event occurred on 15 July 2013 with $M_w = 7.3$, at 21.5 km depth, approximately 100 km east of the triple junction between the South American, Sandwich and Antarctica plates (Fig. 4b). In the South Scotia Ridge transform plate boundary, two strike–slip events took place on 16 and 17 November 2013. The first one was a $M_w = 6.9$ event that occurred at a shallow depth of 10 km. The second one, $M_w = 7.8$, which occurred at a depth of 23.8 km, represents the largest strike–slip earthquake known to date along this plate boundary (Fig. 4b). Southwest of the Falkland Islands, a strike–slip faulting $M_w = 6.9$ earthquake happened on 25 November 2013, near the boundary of the South American and the Scotia Sea plates (Fig. 4b). On 15 April 2014, a $M_w = 6.8$ earthquake occurred in the South Atlantic Ocean to the east of Bouvet Island resulting from strike–slip motion (Fig. 4b).

In the east Mediterranean SZ, two events occurred (Fig. 5). The $M_w = 6.8$ earthquake, which happened on 12 October 2013 about 30 km west of Platanos, Greece, was asso-

ciated with a reverse motion near the Hellenic arc, the region where the African Plate subducts beneath the Aegean Sea Plate (Fig. 5b). The $M_w = 6.9$ earthquake, which occurred on 24 May 2014, was located to the south of Samothraki Island, Greece, near the Saros trough (Fig. 5b), a region with many similar strike–slip earthquakes.

The studied events have different focal mechanisms. Within the total of 23 analyzed earthquakes, 52 % are thrust, 35 % are strike–slip, and 13 % are normal faults. Further information and details on the velocity rate of tectonic plates can be found in DeMets et al. (1994) for the western Pacific SZ, in Angermann et al. (1999) and DeMets et al. (2010) for the eastern Pacific SZ, in DeMets et al. (2010) for the South Atlantic SZ, and in McClusky et al. (2000) for the eastern Mediterranean SZ.

3 Tsunamigenic potential analysis

3.1 Earthquake source models

For each analyzed earthquake event we compute a source model including the fault parameters required for tsunami numerical modeling. For simplification, we adopt a rectangular shape of the fault rupture, characterized by a length (L) and a width (W). We consider the M_w magnitude evaluated by the gCMT for each event and we compute the corresponding dimensions (L and W) using the scaling laws M_w-L/W established by Blaser et al. (2010). In comparison with the most frequently used scaling relations of Wells and Coppersmith (1994), Blaser et al. (2010)'s study has the advantage of considering the subduction zone events in the database that they used to establish the earthquakes' scaling relations.

Once the earthquake fault dimensions (L and W) are calculated, we use the seismic moment (M_o) definition of Aki (1972) (Eq. 1) together with the M_o–M_w relation defined by Kanamori and Anderson (1975) (Eq. 2) in order to calculate the earthquake slip.

$$M_o = \mu \mathrm{LWD} \quad (1)$$

$$M_w = \frac{2}{3} \log M_o - 10.7, \quad (2)$$

where μ is the shear modulus characterizing the rigidity of the earthquake rupture region, and D is the average coseismic fault slip.

Table 1 summarizes the fault parameters computed for all the considered earthquake events. These parameters are used in the next section to compute the tsunami generation.

3.2 Tsunami numerical modeling

In this section, we perform tsunami numerical modeling of both generation and propagation for all considered earthquake events including those observed to trigger tsunamis, and those that did not cause tsunamis. Through tsunami numerical modeling, we attempt to understand why some earthquakes trigger tsunamis and others do not, and how the earthquake source parameters are related to the potential of tsunami generation. Also, by comparing the tsunami observations with the simulations, we aim to discuss how numerical modeling can contribute to a better performance of TWSs.

In order to model tsunami generation and propagation a set of bathymetric/topographic grid data is generated for each region of interest where studied earthquakes took place. 30 arcsec gridded data from the General Bathymetric Chart of the Oceans (GEBCO, 2015) are used in this study.

3.2.1 Tsunami generation

The initial sea-surface perturbation is generated for all the studied earthquakes. The earthquake fault parameters derived in Sect. 3.1 (Table 1) were used to simulate the tsunami generation. The earthquake rupture is supposed instantaneous and the sea-bed displacement is computed using the half-space elastic theory (Okada, 1985). The vertical sea bottom displacement is then transferred to the free ocean surface with the assumption that both deformations of sea bottom and ocean surface are equal (Kajiura, 1970).

Figure 6 depicts the simulated tsunami generation for the 23 earthquake events. Analysis of these results shows a confirmation of tsunami generation for events with recorded tsunami signals (events 9, 11, 14, 15, 16, 18, 19, 21 and 22 in Fig. 6). On the other hand, Okada's tsunami generation modeling, using the fault models elaborated in Sect. 3.1, leads also to non-zero initial sea-surface perturbations for some events with no tsunami observations.

For earthquake events with very deep fault rupture (events 1 and 5), modeling results show no tsunami generation, which is in accordance with the observations and also with reasonable expectations. For the other 21 events that occurred at depths less than 47 km, modeling of tsunami initial conditions shows that tsunamis were generated, while for only nine of them, a tsunami was observed. The computed initial tsunami deformations show higher wave amplitudes for these nine events with tsunami records compared to the other 12 events for which no tsunamis were observed.

Analysis of tsunami generation results (Fig. 6), clearly indicates that the strike–slip events (events: 2, 10, 11, 12, 13, 18, 20 and 23) cause tsunamis with smaller wave amplitudes compared to thrust (events: 3, 4, 8, 14, 15, 16, 17, 21 and 22) and reverse (events: 6, 7 and 19) earthquakes. Among the studied strike–slip earthquakes, events 11 and 18 have more potential of tsunami generation than the rest of events (Fig. 6). For these two events, 11 and 18, tsunami waves of 0.15 and 0.03 m, respectively, were observed (Table 2).

For the thrust and reverse earthquakes, numerical simulations show tsunami generation with relatively significant initial wave amplitudes, ranging from 0.1 m up to about 1 m, especially for the events 15, 16, 19, 21 and 22 (Fig. 6). For these

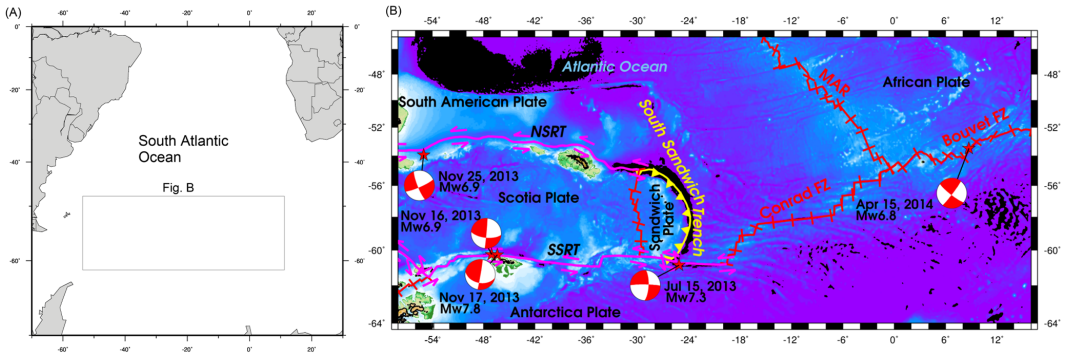

Figure 4. Earthquake events which occurred in the South Atlantic Ocean source zone: **(a)** overview of the source zone; **(b)** location of five events: three around Scotia Plate, one near the Falkland Island and another one near Bouvet Island, their focal mechanisms are strike–slip faulting (red beach ball), the subduction zone (yellow line), the transforms (magenta lines), the active spreading center and fracture zones (red lines).

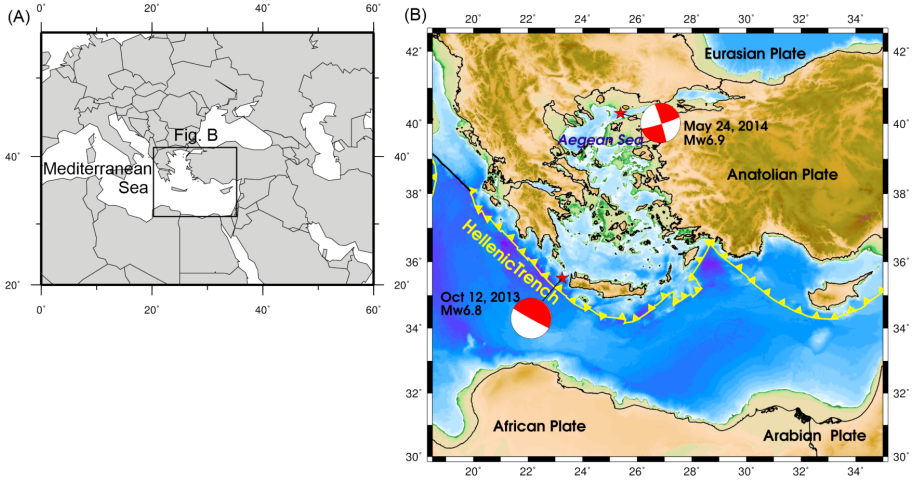

Figure 5. Earthquake events which occurred in the Mediterranean source zone: **(a)** overview of the source zone; **(b)** location of the Greece events (red star), their focal mechanisms: a strike–slip faulting and a reverse faulting (red beach ball), and the subduction zone (yellow line).

earthquakes, tsunami waves of amplitudes between 0.1 m and about 2 m were recorded (Table 2).

Simulations of tsunami generation for studied normal fault earthquakes (events 1, 5 and 9) indicate that only event 9 causes a small initial sea-surface perturbation of about 0.05 m in amplitude (Fig. 6). For the event 9, tsunami waves were recorded with maximum amplitudes of a few centimeters near the source area and of 0.4 m at the coast of Japan (Table 2).

3.2.2 Tsunami propagation

Shallow water equations (SWEs) through the COMCOT code (Liu et al., 1998) are used to simulate the tsunami propagation. This code solves linear and nonlinear SWEs using an explicit staggered leap-frog finite differences numerical scheme for linear terms and an upwind scheme for the nonlinear terms (Wang, 2009). In all considered computation domains, the code employs radiation (or absorbing) boundary conditions, which have the property that the wave motion passes from a domain to the other through the boundaries with no reflections (Broeze and Van Daalen, 1992).

(a) Events with tsunami observations

For all studied tsunamigenic events (39 % of the total events) we perform numerical simulations of tsunami propagation. Here, we present modeling results for the $M_w = 7.1$ Japan event and the $M_w = 8.1$ Chile event that occurred on 25 October 2013 and 1 April 2014, respectively. These events offer a good opportunity to test the reliability of the models considered, including the source model, the bathymetric model and the tsunami propagation code, by comparing the numerical results against the tsunami signals recorded by various DART® stations in the Pacific Ocean.

Table 1. Earthquake parameters for the 23 analyzed events.

Event no.	Date	Epicenter location		Depth (km) (gCMT)	M_w	Location	Fault plane (strike, dip, rake)	L (km)	W (km)	Slip (m)
		Lat. (°)	Lon. (°)							
1	7 Jul 2013	−3.923	153.920	382.9	7.3	Papua New Guinea	167, 47, −70°	77	27	1.83
2	15 Jul 2013	−60.868	−25.144	21.5	7.3	South Sandwich Islands	271, 85, −18°	96	19	2.21
3	30 Aug 2013	51.537	−175.230	26.7	7.0	Aleutian Islands	64, 67, 86°	42	23	1.24
4	25 Sep 2013	−15.838	−74.511	46.1	7.0	Peru	307, 31, 84°	42	23	1.61
5	1 Oct 2013	53.200	152.786	585.5	6.7	Sea of Okhotsk	293, 40, −44°	38	16	0.82
6	12 Oct 2013	35.514	23.252	15.0	6.8	Greece	339, 3, 130°	32	18	0.98
7	15 Oct 2013	9.880	124.117	12.0	7.1	Philippines	42, 40, 80°	47	25	1.54
8	16 Oct 2013	−6.446	154.931	45.8	6.8	Papua New Guinea	307, 43, 85°	32	18	1.04
9	25 Oct 2013	37.156	144.661	24.9	7.1	Japan	171, 43, −107°	60	23	1.56
10	16 Nov 2013	−60.263	−47.062	10.0	6.9	Scotia Sea	96, 66, 2°	53	14	1.13
11	17 Nov 2013	−60.274	−46.401	23.8	7.8	Scotia Sea	102, 44, 3°	200	28	3.40
12	25 Nov 2013	−53.945	−55.003	16.0	6.9	Falkland Islands	158, 80, −171°	53	14	1.34
13	10 Mar 2014	40.829	−125.134	15.0	6.9	California	230, 86, −2°	53	14	1.27
14	16 Mar 2014	−19.981	−70.702	12.0	6.7	Chile	284, 26, 54°	28	17	0.90
15	1 Apr 2014	−19.610	−70.769	21.6	8.1	Chile	355, 15, 106°	177	73	4.00
16	3 Apr 2014	−20.572	−70.502	28.7	7.7	Chile	358, 14, 103°	104	48	3.26
17	11 Apr 2014	−6.586	155.048	44.1	7.1	Papua New Guinea	310, 42, 87°	47	25	1.40
18	12 Apr 2014	−11.270	162.148	27.3	7.6	Solomon Islands	17, 63, 159°	149	24	3.00
19	13 Apr 2014	−11.463	162.051	37.5	7.4	Solomon Islands	91, 43, 77°	70	35	2.42
20	15 Apr 2014	−53.497	8.722	16.4	6.8	Bouvet Island	128, 81, 5°	46	13	1.19
21	18 Apr 2014	17.397	−100.972	18.9	7.3	Mexico	303, 18, 98°	62	31	1.71
22	19 Apr 2014	−6.755	155.024	36.0	7.5	Papua New Guinea	311, 35, 87°	80	39	2.44
23	24 May 2014	40.289	25.389	12.0	6.9	Greece	73, 85, −177°	53	14	1.08

Figures 7 and 8 depict, respectively, the results of tsunami numerical modeling for the $M_w = 7.1$ Japan and the $M_w = 8.1$ Chile events. The results clearly indicate that a tsunami was generated close to the source areas, with wave amplitude of a few centimeters (~ 3 cm) for the Japan event and up to 1 m for the $M_w = 8.1$ Chile event (Figs. 7a and 8a).

Comparison of the simulated tsunami waveforms and the recorded signals from the DART® sensors (Fig. 7b and c for the Japan event, and Fig. 8b–d for the Chile event) shows relatively good agreement in terms of tsunami arrival time and maximum wave amplitudes. In Fig. 7b and c we display the comparison between the simulated waveforms and the ones recorded by the DART®-21346 and the DART®-21418. The analysis of these results clearly shows good agreement between simulated and recorded signals in terms of the tsunami arrival time, wave amplitudes and periods, in spite of the fact that the generated tsunami is relatively small and also both DART® records show first-arrival perturbations with maximum wave amplitudes between 0.5 and 1 cm. We interpret these small oscillations as effects resulted from the filtering process of the DART®-recorded signal. In Fig. 8b we plot both recorded and simulated waveforms for the DART®-32401 station that is located about 290 km west from the earthquake epicenter. The analysis of the sensor record (blue curve) indicates that the DART® station captured, few seconds after the event occurrence, the seismic signal due to its location relatively close to the epicenter. A few minutes later, the DART®-32401 recorded the arrival of the first tsunami wave (Fig. 8b). Simulated waveform (red curve) shows a good agreement with the tsunami recorded signal for both the tsunami travel time of about 18 min and the maximum wave amplitude of about 0.25 m. Figure 8c and d depict the comparison between the recorded and the simulated tsunami signals for both DART® 32412 and 32413, respectively. These sensors are located 1600 and 2800 km far away from the earthquake epicenter and therefore recorded only small tsunami amplitudes (max. amplitude of about 6 cm for DART®-32412, and about 3 cm for DART®-32413 – blue signals in Fig. 8c and d). The simulated waveforms at the locations of DART®-32412 and DART®-32413 (red signals in Fig. 8c and d) also indicate small recorded tsunami amplitudes, relatively in agreement with the recorded ones.

(b) Events with no tsunami observations

Considering the results of tsunami generation presented in Sect. 3.2.1, we model tsunami propagation for events with no tsunami observations but for which Okada's model led to non-zero initial deformations (see Fig. 6). Here, we consider the $M_w = 6.9$ northern Aegean earthquake which occurred on 24 May 2014 as an example to present results of tsunami propagation simulations.

Table 2. Timeline of the actions and activities taken by the considered TWC's for the 23 earthquakes. The font corresponds to the level of tsunami alert (information: Roman, advisory: bold, and warning: italic). MWA is the maximum wave amplitude recorded.

Event, date and origin time (UTC)	Tsunami Warning Agency actions and activities	Tsunami occurrence
Papua New Guinea earthquake ($M_w = 7.3$) 7 Jul 2013 18:35:30	PTWC (at 18:42) issues Tsunami Bulletin 1: information. PTWC Hawaii (at 18:42) issues Tsunami Information Statement 1. ITEWC (at 18:45) issues Tsunami Bulletin 1.	No
South Sandwich earthquake ($M_w = 7.3$) 15 Jul 2013 14:03:43	PTWC Caribbean Sea (at 14:18) issues Tsunami Information Statement 1. ITEWC (14:19) issues Tsunami Bulletin 1.	No
Aleutian Islands earthquake ($M_w = 7.0$) 30 Aug 2013 16:25:02	WC/ATWC (at 16:31) issues Tsunami Information Statement 1. PTWC Hawaii (at 16:34) issues Tsunami Information Statement 1 ($M_w = 6.8$). PTWC issues Tsunami Bulletin 1 (at 16:34): information ($M_w = 6.8$), and Tsunami Bulletin 2: information (at 16:43) ($M_w = 7.0$).	No
Peru earthquake ($M_w = 7.0$) 25 Sep 2013 16:42:43	PTWC issues Tsunami Bulletin 1 (at 16:48): information ($M_w = 6.8$), and Tsunami Bulletin 2 (at 17:11): information ($M_w = 7.2$). WC/ATWC (at 16:49) issues Tsunami Information Statement 1 ($M_w = 6.8$).	No
Sea of Okhotsk earthquake ($M_w = 6.7$) 1 Oct 2013 03:38:21	ITEWC (at 3:48) issues Tsunami Bulletin 1.	No
Greece earthquake ($M_w = 6.8$) 12 Oct 2013 13:11:53	**NOA (at 13:19) issues Tsunami Message 1: information ($M_w = 6.3$).** **ITEWC (at 13:20) issues Tsunami Bulletin 1.** **KOERI issues Tsunami Message 1 (at 13:25): regional watch/advisory ($M_w = 6.8$), Tsunami Message 2 (at 13:42): watch/advisory ($M_w = 6.4$), and watch/advisory cancellation (at 13:57).**	No
Philippines earthquake ($M_w = 7.1$) 15 Oct 2013 00:12:32	PTWC (at 00:22) issues Tsunami Bulletin 1: Information ($M_w = 7.2$). WC/ATWC (at 00:23) issues Tsunami Information Statement 1 ($M_w = 7.2$). JATWC (at 00:24) issues Tsunami Bulletin: Information ($M_w = 7.3$). ITEWC (at 00:24) issues Tsunami Bulletin 1.	No
Papua New Guinea earthquake ($M_w = 6.8$) 16 Oct 2013 10:30:58	PTWC (at 10:37) issues Tsunami Bulletin 1: information ($M_w = 7.1$). ITEWC (at 10:41) issues Tsunami Bulletin 1. JATWC (at 10:46) issues Tsunami Bulletin: information ($M_w = 7.2$).	No
Japan earthquake ($M_w = 7.1$) 25 Oct 2013 17:10:19	**JMA (at 17:14) issues Tsunami Advisories for Fukushima in Japan ($M_w = 6.8$), updated Tsunami Advisories for other coastal regions of Japan ($M_w = 7.1$) (at 17:50), and Tsunami warnings/advisories cancellation message (at 19:05), and information message with Initial Tsunami Observations (at 19:11) Ofunato 0.2 m; Kuji-ko 0.4 m; Ishinomaki-shi Ayukawa 0.3 m; Soma 0.4 m.** **PTWC (at 17:20) issues Tsunami Bulletin 1: information ($M_w = 7.5$).**	Yes (MWA of 0.4 m)

Table 2. Continued.

Event, date and origin time (UTC)	Tsunami Warning Agency actions and activities	Tsunami occurrence
Scotia Sea earthquake ($M_w = 6.9$) 16 Nov 2013 03:34:31	PTWC Caribbean Sea (at 03:43) issues Tsunami Information Statement 1 ($M_w = 7.4$), and Tsunami Information Statement 2 ($M_w = 6.8$) (at 03:53). ITEWC (at 03:48) issues Tsunami Bulletin 1.	No
Scotia Sea earthquake ($M_w = 7.8$) 17 Nov 2013 09:04:55	ITEWC (at 09:16) issues Tsunami Bulletin 1. PTWC (at 09:17) Tsunami Bulletin 1: information. PTWC Caribbean Sea (at 09:18) issues Tsunami Information Statement 1. WC/ATWC (at 09:20) issues Tsunami Information Statement 1. (NOAA reported Tsunami Observations: King Edward TD: 0.15 m).	Yes (MWA of 0.15 m)
Falklands Islands earthquake ($M_w = 6.9$) 25 Nov 2013 06:27:33	PTWC Caribbean Sea (at 06:41) issues Tsunami Information Statement 1 ($M_w = 6.6$) ITEWC (at 06:42) issues Tsunami Bulletin 1.	No
California earthquake ($M_w = 6.9$) 10 Mar 2014 05:18:13	PTWC (at 05:26) Tsunami Bulletin 1: information ($M_w = 7.0$). PTWC Hawaii (at 05:27) issues Tsunami Information Statement 1 ($M_w = 7.0$).	No
Chile earthquake ($M_w = 6.7$) 16 Mar 2014 21:16:29	PTWC (at 21:23) issues Tsunami Bulletin 1: information ($M_w = 7.0$), and Tsunami Bulletin 2 (at 22:26): information with Tsunami Observations: Patache 0.28 m. PTWC Hawaii (at 21:23) issues Tsunami Information Statement 1 ($M_w = 7.0$).	Yes (MWA of 0.28 m)
Chile earthquake ($M_w = 8.1$) 1 Apr 2014 23:46:47	*PTWC (at 23:55) issues Tsunami Bulletin 1: regional Warning/Watch ($M_w = 8.0$), Tsunami Bulletin 2: regional Warning/Watch update and Tsunami Observations: Pisagua 1.92 m; Iquique 1.70 m (at 00:14), Tsunami Bulletin 3: regional Warning/Watch ($M_w = 8.2$) and Tsunami Observations (at 00:34), Tsunami Bulletin 4: regional Warning/Watch and Tsunami Observations (at 01:31), Tsunami Bulletin 5: Warning area reduced (Chile and Peru), Warning/Watch Cancellation for all previously named areas and Tsunami Observations (at 02:35), Tsunami Bulletin 6 (at 03:44): Warning for Chile and Peru and Tsunami Observations: Juan Fernandez 0.16 m; San Felix 0.68 m; Coquimbo 0.15 m; Caldera 0.11 m; Charnal 0.24 m; Callao La-Punta Pe 0.12 m; Arica 1.83 m; Matarani 0.58 m; Paposo 0.26 m; Pisagua 2.01 m; Mejillones 0.86 m; Tocopilla 0.42 m; DART® 32402 0.05 m; Antofagasta 0.25 m; Patache 1.51 m; Iquique 2.11 m, and Tsunami Bulletin 7 (at 04:43): Warning/Watch Cancellation.* *PTWC Hawaii (at 23:56) issues Tsunami Information Statement 1 ($M_w = 8.0$), and Tsunami Advisory for Hawaii with Observations (at 03:46).*	Yes (MWA of 2.11 m)
Chile earthquake ($M_w = 7.7$) 3 Apr 2014 02:43:11	*PTWC (at 02:51) issues Tsunami Bulletin 1: Information ($M_w = 7.4$), Tsunami Bulletin 2: Warning for Chile and Peru ($M_w = 7.8$) (at 03:13), and Tsunami Bulletin 3 (at 03:59): Warning Cancellation and Tsunami Observations: Patache 0.68 m; Pisagua 0.19 m; Iquique 0.74 m.* *PTWC Hawaii (at 02:52) issues Tsunami Information Statement 1 ($M_w = 7.4$).*	Yes (MWA of 0.74 m)

Table 2. Continued.

Event, date and origin time (UTC)	Tsunami Warning Agency actions and activities	Tsunami occurrence
Papua New Guinea earthquake ($M_w = 7.1$) 11 Apr 2014 07:07:23	PTWC (at 07:15) issues Tsunami Information Bulletin 1 ($M_w = 7.3$). ITEWC (at 07:17) issues Tsunami Bulletin 1. JATWC (at 07:19) issues Information Bulletin ($M_w = 6.9$).	No
Solomon Islands earthquake ($M_w = 7.6$) 12 Apr 2014 20:14:39	*PTWC (at 20:20) issues Tsunami Bulletin 1: regional Warning/Watch ($M_w = 8.3$), Tsunami Bulletin 2 (at 20:35): Warning area reduced ($M_w = 7.8$), Tsunami Bulletin 3 (at 20:53): same Warning area ($M_w = 7.6$), and Tsunami Bulletin 4 (at 21:36): Warning Cancellation and Tsunami Observations: DART® 55 012 0.02 m; Lata Wharf 0.03 m.* *ITEWC (at 20:54) issues Tsunami Bulletin 1.*	Yes (MWA of 0.03 m)
Solomon Islands earthquake ($M_w = 7.4$) 13 Apr 2014 12:36:19	*ITEWC (at 12:45) issues Tsunami Bulletin 1.* *PTWC (at 12:46) issues Tsunami Bulletin 1: regional Warning ($M_w = 7.7$), Tsunami Bulletin 2 (at 13:18): Warning area reduced ($M_w = 7.4$), Tsunami Bulletin 3 (at 13:55): Warning area reduced and Tsunami Warning Cancellation for Vanuatu and Papua New Guinea ($M_w = 7.4$), and Tsunami Bulletin 4 (at 14:42): Warning Cancellation and Tsunami Observations: Lifou New Caledonia 0.16 m; Honiara 0.02 m; DART® 55012 0.01 m; Lata Wharf 0.03 m.*	Yes (MWA of 0.16 m)
Bouvet Islands earthquake ($M_w = 6.8$) 15 Apr 2014 03:57:01	PTWC Caribbean Sea (at 04:10) issues Tsunami Information Statement 1. ITEWC (at 04:11) issues Tsunami Bulletin 1.	No
Mexico earthquake ($M_w = 7.3$) 18 Apr 2014 14:27:24	ITEWC (at 14:38) issues Tsunami Bulletin 1 PTWC (at 14:39) issues Tsunami Bulletin 1: Information ($M_w = 7.4$) PTWC Hawaii (at 14:40) issues Tsunami Information Statement 1 ($M_w = 7.4$) NOAA reported Tsunami Observations: Acapulco TD: 0.43 m.	Yes (MWA of 0.43 m)
Papua New Guinea earthquake ($M_w = 7.5$) 19 Apr 2014 13:28:00	*PTWC (at 13:37) issues Tsunami Bulletin 1: regional Warning/Watch ($M_w = 7.8$), Tsunami Bulletin 2 (at 14:18): same Warning area ($M_w = 7.5$), Tsunami Bulletin 3 (at 14:39): Warning Cancellation and Tsunami Observations: Tarekukure Wharf 0.05 m.* *PTWC Hawaii (at 13:40) issues Tsunami Information Statement 1 ($M_w = 7.8$).* *ITEWC* (at 13:40) issues Tsunami Bulletin 1.	Yes (MWA of 0.05 m)
Greece earthquake ($M_w = 6.9$) 24 May 2014 09:25:02	**NOA (at 09:30) issues Tsunami Information Message 1 ($M_w = 6.0$).** **KOERI (at 09:43) issues Tsunami Message 1: regional Watch/Advisory ($M_w = 6.6$), Tsunami Message 2 (at 09:56): Watch Cancellation, and Tsunami Message 3 (at 12:39): Watch/Advisory Cancellation.**	No

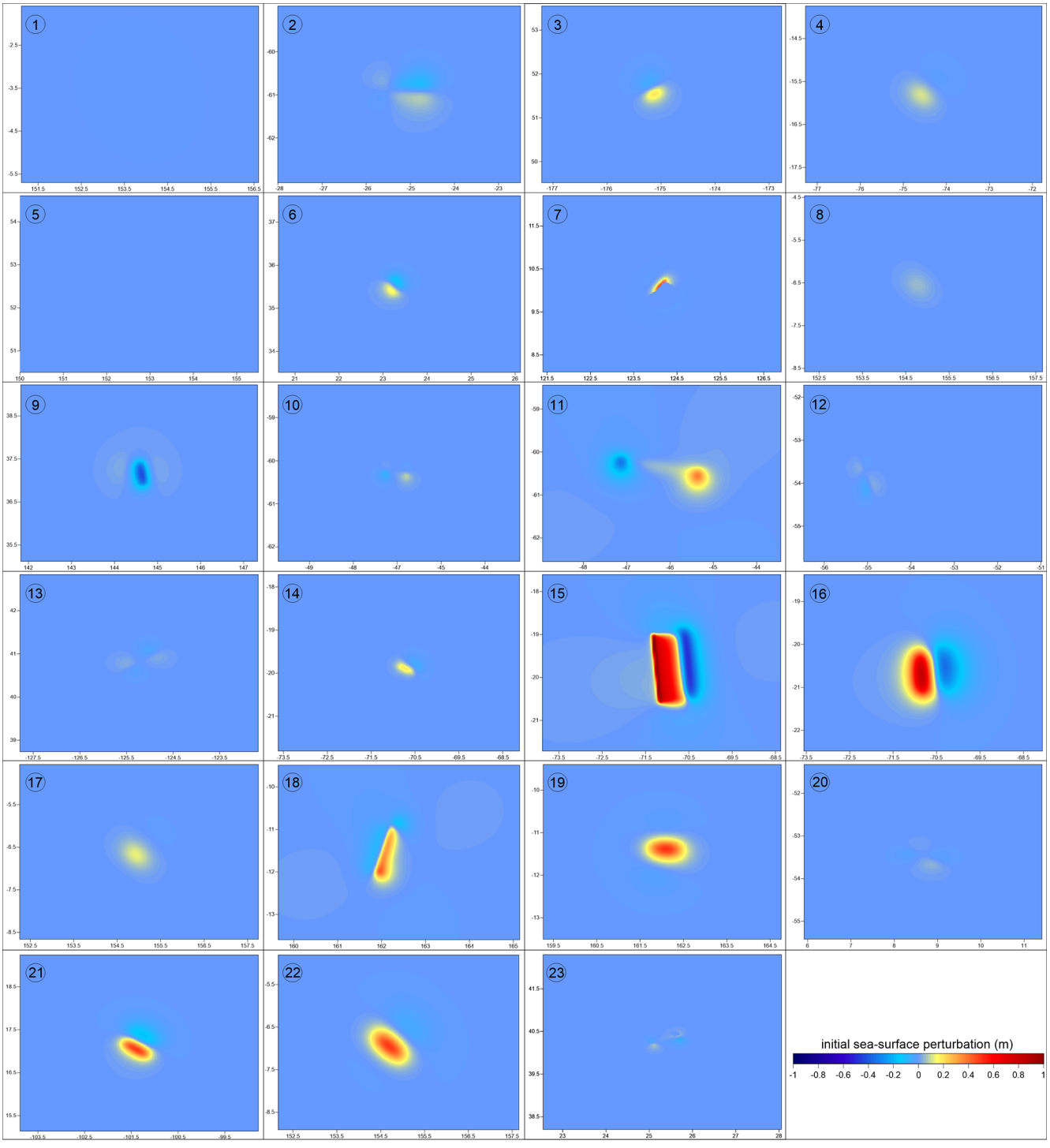

Figure 6. Simulated initial sea-surface perturbations caused by the studied 23 submarine earthquakes. The number in the top-left corner of each figure corresponds to the event's number indicated in Table 1.

Figure 9 depicts both the initial sea-surface perturbation (Fig. 9a) and the maximum wave amplitudes (Fig. 9b) simulated following the occurrence of the $M_w = 6.9$ northern Aegean earthquake. In spite of the fact that no tsunami was recorded in the eastern Mediterranean region after the 24 May 2014 earthquake, modeling the tsunami generation (Fig. 9a) shows the occurrence of a small tsunami with wave amplitude reaching about 7 cm. Along the north Aegean Sea coasts, the computed maximum wave amplitudes range from

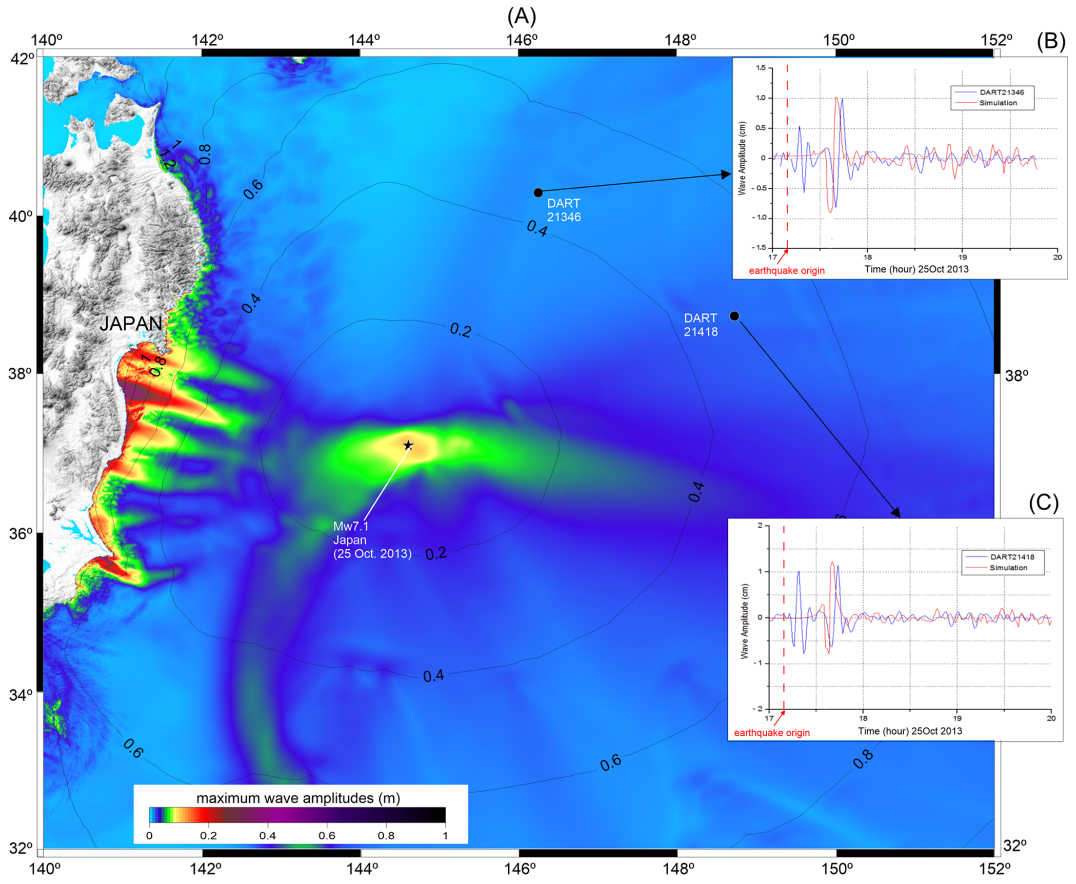

Figure 7. Tsunami numerical simulation of the 25 October 2013 Japan tsunami event: **(a)** maximum wave amplitudes distribution in the west Pacific Ocean and tsunami travel times (dark lines separated each 0.2 h); **(b)** comparison between the simulated waveform and recorded signal for the station DART®-21346; **(c)** comparison between the simulated waveform and recorded signal for the station DART®-21418.

a few centimeters up to about 0.15 m, reaching a maximum in some coastal zones of the region.

4 Discussion

4.1 Tsunami numerical modeling

Tsunami numerical modeling is a key component of any end-to-end tsunami warning system. Recent progress in numerical modeling allows estimates of tsunami generation, propagation and coastal impact in a proper way, reaching good agreement with the recorded and observed data. In this study, we employ a simple earthquake source model, available bathymetric model and a validated shallow water code for tsunami simulations.

4.1.1 Tsunami generation

Simulations of tsunami generation are performed using regression laws to retrieve the fault dimension and the average coseismic slip from the earthquake magnitude, and then employing the half-space elastic theory of Okada (1985) to compute the sea-bed deformation. Tsunami initial condition results (Fig. 6) show relatively significant sea-surface deformations for events with recorded tsunamis but also lead to small initial perturbation for some events with no tsunami observations.

Tsunami generation results highlight, on the one hand, the importance of the earthquake focal mechanism in controlling the tsunamigenic potential, and on the other hand, the limitation of the used generation model. Comparing the tsunami initial deformations of both events 11 and 16 of strike–slip and thrust focal mechanism, respectively, and of relatively similar magnitudes and depths, clearly indicates that the thrust fault has more potential of tsunami generation than the strike–slip. However, the tsunami potential is not only determined by the focal mechanism because some events seem to have focal mechanisms that favor the result of tsunamis, but for which no waves were observed. The reverse $M_w = 7.1$ earthquake that occurred in the Philippines at a depth of 12 km (event 7) illustrates an example of these events.

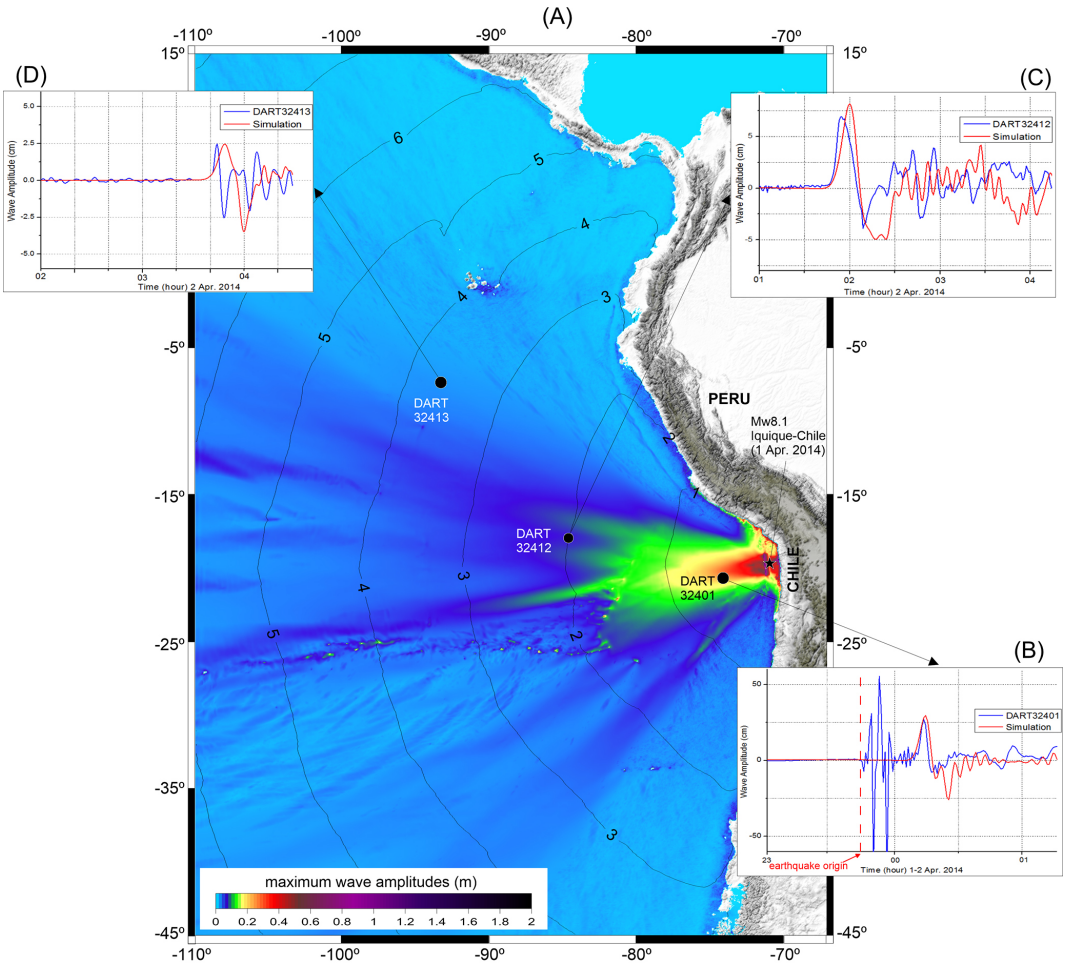

Figure 8. Tsunami numerical simulation of the 1 April 2014 Iquique-Chile tsunami event: **(a)** maximum wave amplitudes distribution in the east Pacific Ocean and tsunami travel times (dark lines separated each 1 h); **(b)** comparison between the simulated waveform and recorded signal for the station DART®-32401; **(c)** comparison between the simulated waveform and recorded signal for the station DART®-32412; **(d)** comparison between the simulated waveform and recorded signal for the station DART®-32413.

Another important factor that seems to affect tsunami generation is the specific location of some events in oceanic/sea regions characterized by the presence of islands. The presence of the islands in the co-seismically deformed region of an earthquake can significantly reduce its tsunamigenic potential. The 15 October 2013, $M_w = 7.1$, earthquake in the Philippines (event 7) and the 24 May 2014, $M_w = 6.9$, northern Aegean earthquake (event 23) are two events for which the co-seismically deformed areas include islands. This may be why no tsunami was recorded for these two events, even though the numerical modeling shows the generation of small tsunamis (see Fig. 6).

Simulation results (Fig. 6) led to the generation of tsunamis for 21 earthquake events, while for only nine events, tsunamis were observed. The results (Fig. 6) also show that the computed initial sea-surface deformations with relatively significant wave amplitudes correspond to the cases with observed tsunamis. For almost all the other events, initial waves of a few centimeters were simulated. For some events, considered as non-tsunamigenic, the associated earthquakes might trigger small tsunamis, as simulated in Fig. 6, but they were not recorded due to the absence of sensors in the near-field areas. Events 2, 10 and 20 are examples of such earthquakes.

The simulation results highlight the relative limitation of the source model calculations considered in this study that retrieved the fault dimension and average coseismic slip from the earthquake magnitude using empirical scaling laws. Moreover, assuming a uniform slip distribution along the fault plane may result in inappropriate estimates of the tsunami initial wave. A better constraint of the source model and slip distribution requires inversion methods of both seismic and tsunami data. Although these methods are robust for the source model evaluation, they are less appropriate for early tsunami warning purposes that are usually based on fast estimates of source parameters.

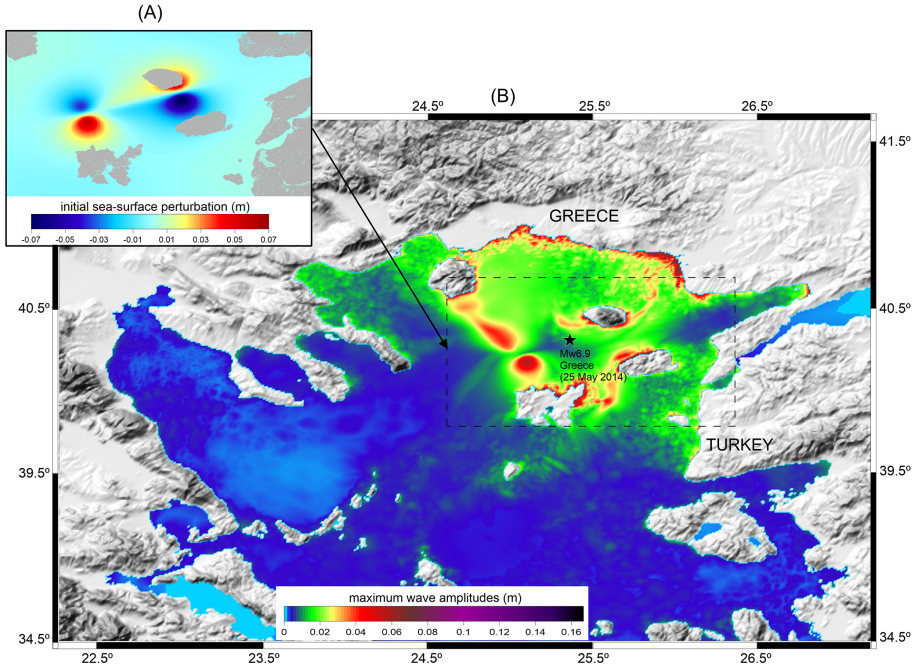

Figure 9. Tsunami numerical simulation of the $M_w = 6.9$ northern Aegean earthquake which occurred on 24 May 2014: **(a)** tsunami generation; **(b)** maximum wave amplitudes distribution in the north Aegean Sea.

4.1.2 Tsunami propagation

The results of tsunami numerical modeling for both the $M_w = 7.1$ Japan and the $M_w = 8.1$ Chile events that occurred on 25 October 2013 and 1 April 2014, respectively (Figs. 7 and 8), produced relatively good estimates of wave amplitudes and arrival times when compared with the recorded signals from DART® stations. These two cases indicate that the expeditious strategy involving Okada-like modeling of the tsunami initial condition and numerical modeling of the tsunami propagation can produce correct results. Nevertheless, the lack of precise source information (dimension and slip) and detailed bathymetric models leads to some differences between these signals. Figures 7b, c and 8b–d highlight these limitations, especially regarding the estimates of the wave periods and the amplitudes of the second waves. This is particularly due to the use of empirical scaling law to estimate the earthquake fault parameters (dimension and slip) as well as adopting a uniform slip distribution along the fault plane. Appropriate methods to constrain the fault slip distribution model require inversion of tsunami data (Fujii et al., 2011; Wei et al., 2013; Satake et al., 2013).

An et al. (2014) assessed the source model of the 1 April 2014 tsunami using the least square inversion of tsunami records from three DART® stations in the Pacific Ocean. Considering this source model they were able to properly reproduce the tsunami waveforms at the stations locations using a shallow water model. Their approach is robust in constraining the earthquake source model from tsunami observations. However, for early tsunami warning purposes a fast estimate of the earthquake source is essential. Tsunami data inversion requires the use of at least the complete first wave, which leads to delays in tsunami warning dissemination that can be significant, especially for local and regional events.

On the other hand, tsunami numerical results for the Mw6.9 north Aegean earthquake (Fig. 9) show the occurrence of a small tsunami, maximum wave amplitudes reaching about 0.15 m, in the absence of any record or observation. This fact clearly highlights the limitation of the regression laws used in this study to retrieve the fault dimension and the average coseismic slip from the earthquake magnitude only. Also, the presence of the islands in the co-seismically deformed region of the north Aegean earthquake can be one of the factors that determined the tsunamigenic potential of the event.

In spite of these limitations related to the models used (earthquake source model, bathymetric model and the shallow water code), they present the advantage of fast estimates of the earthquake source parameters and then a fast computation of the tsunami threat, which is relevant for any TWS in particular for the case of local and regional tsunamigenic hazardous source zones. However, in some cases the considered models can lead to inappropriate estimates of tsunami hazards and therefore to inappropriate tsunami warning decisions.

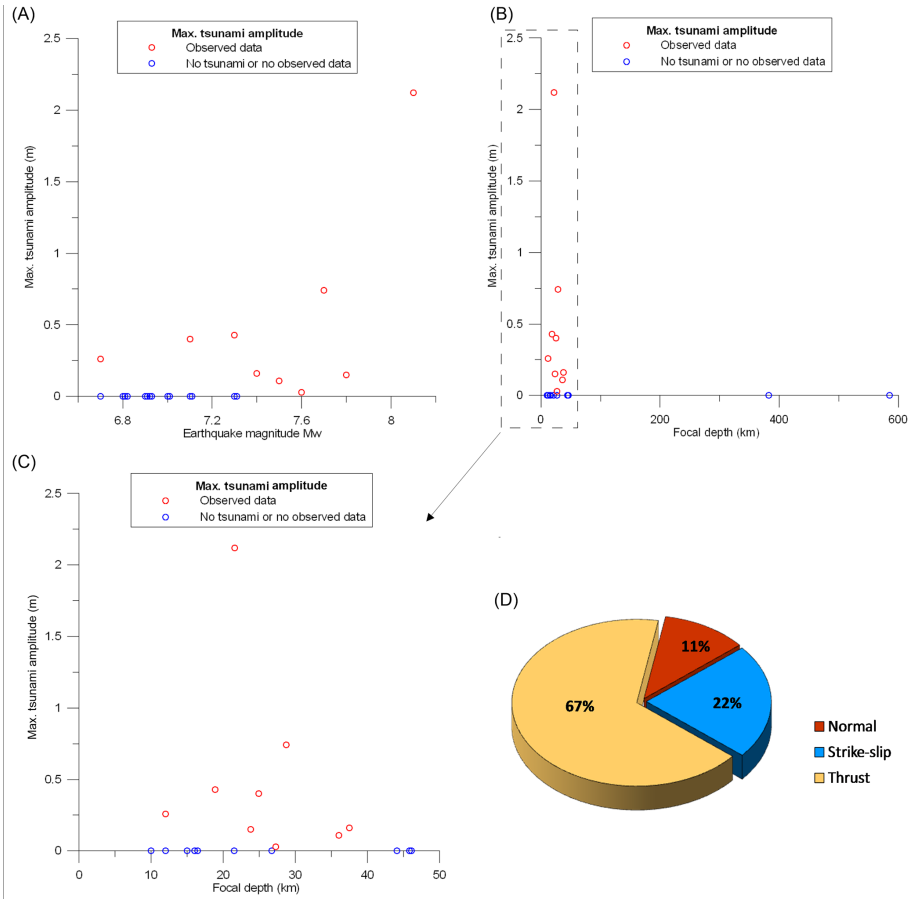

Figure 10. (a) Observed tsunami wave amplitudes for the various magnitudes of the analyzed earthquakes; **(b)** observed tsunami wave amplitudes for the different depths of the analyzed events; **(c)** zoom on the depth region from 0–50 km and the corresponding observed tsunami wave amplitudes; **(d)** proportions of mechanism focal types for the earthquake events that caused tsunamis.

4.2 Tsunamigenic potential and sensitivity to earthquake parameters

In addition to the magnitude, two main parameters are recognized to control the tsunamigenic potential, namely the focal mechanism and the rupture depth. Here, we focus only on events with confirmed tsunami and we discuss the sensitivity of tsunami generation and potential to these three parameters.

The studied events occurred with magnitudes ranging from $M_w = 6.7$ up to 8.1, at depths between 10 and 585 km, with various focal mechanisms that include normal, strike–slip and thrust faults. 39 % of these earthquakes triggered tsunamis that were confirmed from DART® and/or TD records.

In order to highlight the sensitivity of tsunami potential to earthquake parameters, we plot in Fig. 10 the observed tsunami wave amplitudes for the different earthquake magnitudes and rupture depths, as well as the proportion of mechanism focal types for tsunamigenic events. Figure 10a depicts the observed tsunami wave amplitudes for the various earthquake magnitudes. This figure indicates that higher wave amplitude (more than 2 m) was observed for higher earthquake magnitude ($M_w = 8.1$). However, higher magnitude does not always cause the higher tsunami waves, because the figure also shows that in some cases, higher magnitude earthquake events (the $M_w = 7.6$ Solomon Islands earthquake) cause lower tsunami amplitudes than smaller magnitude events (the $M_w = 6.7$ Chile earthquake). This fact clearly indicates that the event magnitude is not the only factor controlling the tsunami potential, but there are other parameters of significant importance. In Fig. 10b and c, we plot observed tsunami wave amplitudes for the different depths of the analyzed events. These figures show that significant tsunamis were recorded for low depths. In Fig. 10d we plot the proportions of mechanism focal types in order to highlight the contribution of each rupture type to the tsunamigenic potential. As expected, Fig. 10d shows clearly that most tsunami events (67 %) were due to reverse/thrust earthquake fault ruptures. This is due to the fact that the dip-slip faults, including normal and reverse ruptures, are the favorite earthquake mechanisms for tsunami generation more than the strike–slip ones as they induce more substantial vertical displacement of the

ocean bottom; although, the strike–slip earthquakes may also trigger tsunamis, in particular when they present a dip-slip component or when they interact with irregular sea-bottom topography (Tanioka and Satake, 1996).

A number of research studies have investigated the sensitivity of tsunamigenic potential to earthquake parameters. Okal (1988) showed that the primary parameter affecting tsunami generation is the seismic moment. Geist and Yoshioka (1996) studied the source parameters controlling the generation of tsunamis along the Cascadia margin. They concluded that the major factors influencing the generation of tsunamis are the shallowness of the rupture and the type of the fault. These studies are in relatively good agreement with our results since most confirmed tsunamis are caused by events of large magnitude occurring at shallow depths with thrust/reverse faulting ruptures.

It is important to mention here that among the studied events, some of them are non-tsunamigenic, even though they seem able to cause tsunamis due to their shallow rupture. Such events can lead to the dissemination of false alerts especially when the TWS is based upon a pre-defined decision matrix. The events which occurred in the Mediterranean Sea ($M_w = 6.8$ Hellenic and $M_w = 6.9$ Aegean events) clearly illustrate the limitation of the use of decision matrix that is usually based only upon earthquake parameters (magnitude, depth and location) to estimate the severity of the tsunami. This is in accordance with the study by Tinti et al. (2012) who investigated the limitation of the decision matrix for the NE Atlantic, Mediterranean and connected seas (NEAM) region, showing the importance of considering additional earthquake characteristics such as the focal mechanism.

4.3 Tsunami warning

The main goal of a TWC is to provide early alerts to the endangered coastal population when a possible tsunami is generated. Depending of the severity of the occurred earthquake and the subsequent tsunami, four types of warning messages are used by the TWCs around the world including warning, advisory, watch and information. The tsunami warning message includes, in general, information on earthquake parameters (origin time, location, depth and magnitude) as well as an evaluation of the tsunami threat in the surrounding coasts.

For the 23 earthquake events, analyzed in this paper, tsunami alerts were issued by various TWCs (international, regional, national and/or local) including the Pacific Tsunami Warning Center (PTWC), the West Coast/Alaska Tsunami Warning Center (WC/ATWC), the Japan Meteorological Agency (JMA), the Joint Australian Tsunami Warning Center (JATWC), the Indian Tsunami Early Warning Centre (ITEWC), and the three candidate tsunami watch providers of the NEAM region, namely the National Observatory of Athens (NOA), Kandilli Observatory and Earthquake Research Institute (KOERI) and the tsunami warning center at the National Institute of Geophysics and Volcanology, Rome ("Centro di Allerta Tsunami" at "Istituto Nazionale di Geofisica e Vulcanologia": CAT-INGV). Alert messages of warning type were issued for 39 % of these events. Warning level messages were disseminated by the PTWC for five earthquake events that occurred in Chile ($M_w = 8.1$ and $M_w = 7.7$), in the Solomon Islands ($M_w = 7.6$ and $M_w = 7.4$), and in Papua New Guinea ($M_w = 7.5$). Watch/advisory level messages were issued by JMA for the $M_w = 7.1$ earthquake that occurred in Japan and by KOERI for both the $M_w = 6.8$ Hellenic and the $M_w = 6.9$ Aegean events. For the rest of the events, the issued messages were of information type. In Table 2 we summarize, for each studied event, the warning issued data including the disseminated alerts, the agency responsible for alerting, and the type of the alert message.

On the other hand, some of the issued messages can be classified as "false warnings" due to the fact that for some non-tsunamigenic events, alert messages were disseminated indicating possible tsunami generation and coastal impact. The $M_w = 6.8$ Hellenic and the $M_w = 6.9$ Aegean events occurred in the Mediterranean Sea illustrate such cases well. For both events, KOERI had issued regional "watch/advisory" warning messages with possible coastal impact (see Table 2), while it is confirmed later that no tsunami was generated. These kinds of "false alerts" are mainly due to the use of a pre-defined decision matrix with limited earthquake characteristics, as highlighted in Tinti et al. (2012), to estimate the tsunami potential and its severity. Moreover, there was a relatively "missed tsunami alarm" for the $M_w = 7.3$ Mexico event, that caused a 0.43 m amplitude tsunami recorded by Acapulco TD, while PTWC only issued a tsunami information bulletin with no report on the tsunami threat.

Reducing the time delay to issue the first tsunami message after the earthquake occurrence remains challenging for any early TWC. In general, for the analyzed events in this paper, the TWCs have well performed by disseminating early tsunami messages within 10 min after the occurrence of the earthquakes for 75 % of the events. By gathering the tsunami warning messages from the TWCs for the studied events, the proportions of the first message time delay indicate that for 9 % of the events, the first warning message was issued within 2–5 min, for about 70 % of the events within 5–10 min and for less than 22 % of the events, the warning messages were disseminated between 10 and 15 min.

5 Conclusions

This study is a contribution to a better understanding of the tsunami potential from large submarine earthquakes occurring worldwide. The study considered the preliminary parameters evaluated for the earthquake events and the tsunami recorded data and used source evaluation models together with tsunami modeling to investigate the tsunami potential.

The analysis of 23 submarine earthquake events which occurred worldwide with magnitudes ranging from $M_w = 6.7$ up to $M_w = 8.1$ leads to the following conclusions:

1. A significant number of events (39 %) were tsunamigenic.

2. Most earthquake events that cause confirmed tsunamis have, as expected, a combination of source parameters that "favor" tsunami generation, namely a shallow depth and a thrust/reverse faulting focal mechanism that took place on/near the subduction zones.

3. The strike–slip events that trigger tsunamis (11 and 18), with relatively small amplitudes of a few centimeters, are only those of large magnitude ($M_w > 7.5$) which occurred at shallow depth (< 30 km).

4. Most earthquakes that did not trigger tsunamis have fault ruptures that are too deep (events 1 and 5), they present "non-favoring" earthquake focal mechanisms (almost pure strike–slip, events 10, 13) or they occurred in areas with the presence of islands in the coseismically deformed region (events 7 and 23).

5. Simulations of the tsunami generation predicted non-zero initial sea-surface perturbations for some events with non-confirmed tsunamis.

6. Numerical modeling of tsunamis is an important tool for wave amplitude and tsunami travel time estimates and then relevant for any TWS, in spite of some limitations on source evaluation and bathymetric data.

7. TWCs around the world have performed relatively well for the most analyzed cases as they provide first warning within 10 min for more than 78 % of the tsunami events. However for some events, "false alerts" were disseminated, in particular in the Mediterranean Sea ($M_w = 6.8$ Hellenic and the $M_w = 6.9$ Aegean events) where the tsunami warning is mainly based on the use of a predefined decision matrix.

In summary, the present study can help characterize tsunami decision matrixes for the various oceanic regions. Tsunami decision matrixes that are based only on limited earthquake parameters (magnitude, depth and location) should be improved and revised in order to increase the number of the considered earthquake parameters to be taken into account (the focal mechanism, for instance).

Acknowledgements. This work is funded by the Join Research Center (JRC) GTIMS project (Global Tsunami Information Monitoring Service), tender no. JRC/IPR/2013/G.2/13/NC, and by the EU project ASTARTE – Assessment, STrategy And Risk Reduction for Tsunamis in Europe Grant 603839, 7th FP (ENV.2013.6.4-3 ENV.2013.6.4-3). The maps in this work were made using the GMT software package (Wessel et al., 2013), the main tectonic boundaries were from Bird (2003) and the 30 arcsec bathymetry background was from GEBCO (2015).

Edited by: A. Armigliato
Reviewed by: three anonymous referees

References

Aki, K.: Scaling law of earthquake source time-function, Geophys. J. Int., 31, 3–25, 1972.

An, C., Sepúlveda, I., and Liu, P. L. F.: Tsunami source and its validation of the 2014 Iquique, Chile, earthquake, Geophys. Res. Lett., 41, 3988–3994, 2014.

Angermann D., Klotz, J., and Reigber, C.: Space-geodetic estimation of the Nazca-South America Euler vector, Earth Planet. Sc. Lett., 171, 329–334, 1999.

Bird, P.: An updated digital model of plate boundaries, Geochem. Geophy. Geosy., 4, 1027–1080, 2003.

Blaser, L., Krüger, F., Ohrnberger, M., and Scherbaum, F.: Scaling relations of earthquake source parameter estimates with special focus on subduction environment, Bull. Seismol. Soc. Am., 100, 2914–2926, 2010.

Broeze, J. and Van Daalen, E. F. G.: Radiation boundary conditions for the two-dimensional wave equation from a variational principle, Math. Comp., 58, 73–82, 1992.

DeMets, C., Gordon, R. G., Argus, D. F., and Stein, S.: Effect of recent revisions to the geomagnetic reversal time scale on estimates of current plate motions, Geophys. Res. Lett., 21, 2191–2194, 1994.

DeMets, C., Gordon, R. G., and Argus, D. F.: Geologically current plate motions, Geophys. J. Int., 181, 1–80, doi:10.1111/j.1365-246X.2009.04491.x, 2010.

Fujii, Y., Satake, K., Sakai, S. I., Shinohara, M., and Kanazawa, T.: Tsunami source of the 2011 off the Pacific coast of Tohoku Earthquake, Earth Planets Space, 63, 815–820, 2011.

GEBCO – General Bathymetric Chart of the Oceans: available at: http://www.gebco.net/, last access: 1 January 2015.

Geist, E. and Yoshioka, S.: Source parameters controlling the generation and propagation of potential local tsunamis along the Cascadia margin, Nat. Hazards, 13, 151–177, 1996.

Heidarzadeh, M. and Satake, K.: Possible sources of the tsunami observed in the northwestern Indian Ocean following the 2013 September 24 Mw 7.7 Pakistan inland earthquake, Geophys. J. Int., 199, 752–766, 2014.

Kajiura, K.: Tsunami source, energy and the directivity of wave radiation, Bull. Earthq. Res. Inst. Tokyo Univ., 48, 835–869, 1970.

Kanamori, H. and Anderson, D. L.: Theoretical basis of some empirical relations in seismology, Bull. Seismol. Soc. Am., 65, 1073–1095, 1975.

Lagmay, A. M. F. and Eco, R.: Brief Communication: On the source characteristics and impacts of the magnitude 7.2 Bohol earthquake, Philippines, Nat. Hazards Earth Syst. Sci., 14, 2795–2801, doi:10.5194/nhess-14-2795-2014, 2014.

Lay, T., Yue, H., Brodsky, E. E., and An, C.: The 1 April 2014 Iquique, Chile, Mw 8.1 earthquake rupture sequence, Geophys. Res. Lett., 41, 3818–3825, 2014.

Liu, P. L.-F., Woo, S.-B., and Cho, Y.-S.: Computer programs for tsunami propagation and inundation, Technical report, Cornell University, USA, available at: http://tsunamiportal.nacse.org/documentation/COMCOT_tech.pdf (last access: December 2014), 1998.

Hamburger, M., Hurst, K., Kahle, H., Kastens, K., Kekelidze, G., King, R., Kotzev, V.,Lenk, O., Mahmoud, S., Mishin, A., Nadariya, M., Ouzounis, A., Paradissis, D., Peter, Y., Prilepin, M., Reilinger, R., Sanli, I., Seeger, H., Tealeb, A., N. Toksöz, M., and Veis, G.: Global Positioning System constraints on plate kinematics and dynamics in the eastern Mediterranean and Caucasus, J. Geophys. Res.-Solid Ea., 105, 5695–5719, 2000.

NGDC/WDS – National Geophysical Data Center/World Data Service: Global Historical Tsunami Database, National Geophysical Data Center, NOAA, doi:10.7289/V5PN93H7, available at: https://www.ngdc.noaa.gov/hazard/tsu_db.shtml, last access: 10 December 2014.

Okada, Y.: Surface deformation due to shear and tensile faults in a half-space, Bull. Seismol. Soc. Am., 75, 1135–1154, 1985.

Okal, E. A.: Seismic parameters controlling far-field tsunami amplitudes: a review, Nat. Hazards, 1, 67–96, 1988.

Satake, K. and Tanioka, Y.: Sources of tsunami and tsunamigenic earthquakes in subduction zones, in: Seismogenic and Tsunamigenic Processes in Shallow Subduction Zones, Birkhäuser, Basel, 467–483, 1999.

Satake, K., Fujii, Y., Harada, T., and Namegaya, Y.: Time and space distribution of coseismic slip of the 2011 Tohoku earthquake as inferred from tsunami waveform data, Bull. Seismol. Soc. Am., 103, 1473–1492, 2013.

Tanioka, Y. and Satake, K.: Tsunami generation by horizontal displacement of ocean bottom, Geophys. Res. Lett., 23, 861–864, 1996.

Tinti, S., Graziani, L., Brizuela, B., Maramai, A., and Gallazzi, S.: Applicability of the Decision Matrix of North Eastern Atlantic, Mediterranean and connected seas Tsunami Warning System to the Italian tsunamis, Nat. Hazards Earth Syst. Sci., 12, 843–857, doi:10.5194/nhess-12-843-2012, 2012.

Wang, X.: COMCOT user manual-version 1.7, School of Civil and Environmental Engineering, Cornell University Ithaca, New York, USA, http://ceeserver.cee.cornell.edu/pll-group/doc/COMCOT_UserManualv17.pdf (last access: December 2014), 2009.

Wei, Y., Chamberlin, C., Titov, V. V., Tang, L., and Bernard, E. N.: Modeling of the 2011 Japan tsunami: Lessons for near-field forecast, Pure Appl. Geophys., 170, 1309–1331, 2013.

Wells, D. L. and Coppersmith, K. J.: New empirical relationships among magnitude, rupture length, rupture width, rupture area, and surface displacement, Bull. Seismol. Soc. Am., 84, 974–1002, 1994.

Wessel, P., Smith, W. H., Scharroo, R., Luis, J., and Wobbe, F.: Generic mapping tools: improved version released, Eos Trans. Am. Geophys. Un., 94, 409–410, 2013.